Chinese Chemical Letters 34 (2023) 107934

Contents lists available at ScienceDirect

Chinese Chemical Letters

journal homepage: www.elsevier.com/locate/cclet

High-efficiency circularly polarized emission from liquid-crystalline platinum complexes

Peng Fan[a,1], Zhou Fang[a,1], Shengyue Wang[a], Qiwei Dong[a], Chen Xiao[a], Alice J. McEllin[b], Duncan W. Bruce[b,*], Weiguo Zhu[a,**], Yafei Wang[a,c,**]

[a] Jiangsu Key Laboratory of Environmentally Friendly Polymeric Materials, Jiangsu Collaborative Innovation Center of Photovoltaic Science and Engineering, Jiangsu Engineering Laboratory of Light-Electricity-Heat Energy-Converting Materials and Applications, School of Materials Science & Engineering, Changzhou University, Changzhou 213164, China
[b] Department of Chemistry, University of York, York YO10 5DD, United Kingdom
[c] Anhui Sholon New Material Technology Co., Ltd., Chuzhou 239500, China

ARTICLE INFO

Article history:
Received 7 July 2022
Revised 9 October 2022
Accepted 13 October 2022
Available online 27 October 2022

Keywords:
Circularly polarized emission
Liquid-crystalline
Platinum complex
Organic light-emitting diodes

ABSTRACT

Realizing both a high emission efficiency and luminescence dissymmetry factor (g_{lum}) in circularly polarized solution processable organic light-emitting diodes (CP-OLEDs) remains a significant challenge. In this contribution, two chiral phosphorescent liquid crystals based on cyclometalated platinum complexes are prepared, in which the chiral *s*-2-methyl-1–butyl group is introduced into the cyclometalating ligand and the mesogenic fragment is attached to the periphery of the ancillary ligand. The platinum complexes exhibit both smectic and chiral nematic phases as evidenced by polarized optical microscopy, differential scanning calorimetry and small-angle X-ray diffraction. Remarkably, a high photoluminescent quantum efficiency of over 78% and clear circularly polarized luminescent signal with g_{PL} of about 10^{-2} are observed for the complexes. Further, solution-processed CP-OLEDs show maximum external quantum efficiencies (*EQE*) of over 15% and strong circularly polarized electroluminescent signals with a $g_{EL} \approx 10^{-2}$. This research demonstrates that both liquid crystallinity and the number of chiral centers play key roles in improving the chiroptical property, paving the way for a new approach for the design of high-efficiency CPL emitters.

Circularly polarized luminescence (CPL) has attracted much attention in the organic semiconductor field [1], such as liquid crystal display (LCD) panels [2], 3D displays [3], spintronic devices [4] and light-emitting devices [5–7] because of its unique polarization and the ability to distinguish and deliver the information from three dimensions [8]. Usually, the dissymmetry factor (g_{lum}), defined as $2(I_L - I_R)/(I_L + I_R)$, is an essential factor for evaluating the intensity of CPL emission, where I_L and I_R refer to the intensities of left- and right-CP emitted light, respectively [7,9]. Since the first report of a circularly polarized organic light-emitting diode (CP-OLED) by Meijer in 1997 [10], the feature of direct CPL generated by electrical excitation has attracted great attention in both industry and academia [11–17]. Thus, CP-OLED can decrease the loss of brightness and reduce power consumption, both of which usually sharply increase with the additional of the linear polarizer and quarter wave plate common in OLEDs [7]. To date, considerable progresses have been made on CP-OLED including traditional fluorescent, phosphorescent and thermally activated delayed fluorescent (TADF) emitters [5–7,18]. Due to the intrinsically low internal quantum efficiency (25%) of traditional fluorescent molecules [19], chiral phosphorescent/thermally activated delayed fluorescent emitters based CP-OLED have been developed over the past few years due to their full utilization of both singlet and triplet excitons [20–31]. For example, Fuchter and coworkers reported CP-OLEDs based on a chiral platinum helicene emitter with a record g_{EL} value of 0.38 [32], although rather poor device performance was observed for this chiral platinum complex. Zheng and coworkers achieved a very high maximum external quantum efficiency (EQE) of 23.7% with small efficiency roll-off in a chiral iridium-based CP-OLED [33], but the g_{EL} value was very low (*ca.* 10^{-4}).

* Corresponding author.
** Corresponding authors at: Jiangsu Key Laboratory of Environmentally Friendly Polymeric Materials, Jiangsu Collaborative Innovation Center of Photovoltaic Science and Engineering, Jiangsu Engineering Laboratory of Light-Electricity-Heat Energy-Converting Materials and Applications, School of Materials Science & Engineering, Changzhou University, Changzhou 213164, China.
E-mail addresses: duncan.bruce@york.ac.uk (D.W. Bruce), zhuwg18@126.com (W. Zhu), qiji830404@hotmail.com (Y. Wang).
[1] These authors contributed equally to this work.

https://doi.org/10.1016/j.cclet.2022.107934
1001-8417/

Recently, Yang and coworkers prepared a pair of novel chiral iridium complexes containing dual chiral centers [34], which exhibited excellent device performance with a maximum *EQE* of 30.6% and a g_{EL} of 7.7×10^{-3}. Obviously, there remains room for further improving phosphorescent-based CP-OLEDs with both good device performance and g_{EL} value. As an alternative method, thermally activated delayed fluorescence (TADF) become the third-generational emitter in OLED owing to the theoretical 100% internal quantum efficiency and metal-free nature of the materials [35–41], which in turn triggered work into TADF-based CP-OLEDs. Although much progress on TADF-based CP-OLED has been achieved recent years [42–46], the large electric dipole transition moment and small magnetic dipole transition moment in pure organic molecules lead to a relatively low dissymmetry factor [47,48]. In addition, the efficiency roll-off of TADF-based device is severe due to the relatively long emission lifetime. Therefore, it is necessary to develop CPL emitters with both high emission efficiency and high g_{EL}.

Luminescent liquid crystals have the advantages of emission efficiency and long-range order in the condensed state, which are beneficial for developing of efficient OLEDs [49]. Additionally, integration of the liquid crystal into a CPL emitter can effectively amplify the g_{lum} factor [50,51]. With this in mind, previously we prepared platinum-based chiral metallomesogens with the maximum EQE of 12% and g_{EL} of 10^{-2} [51], in which the alkoxy chain with a chiral center was part of the cyclometalating ligand and the mesogenic units were attached to the ancillary-diketonate ligand. Unfortunately, the chiral center of the 2-octanol used in these materials can be subject to racemization during the ligand preparation, which can compromise device performance and g_{EL} values, as well as increases the cost of purification with chiral HPLC. Therefore to address these issues, a simply strategy of modifying the chiral group was proposed and employed in this contribution. The proof-of-concept of the platinum complex was constructed by introducing the chiral *s*-2-methyl-1–butyl chiral moiety to replace *s*-2-octanol, as the former's chiral center is remote from the reaction center suppressing racemization during synthesis. Therefore, a cyclometalated platinum complex, called ***s*-Pt1** (Fig. 1a), with one *s*-2-methyl-1–butyl moiety was prepared and simply purified *via* column chromatography on silica. Then in order to explore the effect of the number of chiral centers, a second complex, ***s*-Pt2**, was prepared containing two *s*-2-methyl-1–butyl groups. Both complexes show mesogenic property and high emission efficiency and a distinct CPL signal with a maximum g_{PL} value of 0.012 was obtained from the annealed film. As expected, the solution processed CP-OLEDs based on this chiral platinum complex achieved a satisfactory *EQE* of over 15% and high g_{EL} of about 10^{-2}.

The synthetic route to the platinum complexes is depicted in Scheme S1 (Supporting information). Starting from commercial *s*-2-methyl-1-butanol and 6-bromopyridin-3-ol, compound **1** was prepared *via* a Mitsunobu reaction in the presence of PPh_3 and diisopropyl azodiformate (DIAD) in THF. This was then reacted with phenylboronic acid in a typical Suzuki-Miyaura coupling to provide the cyclometalating ligand **2** in 83% yield. Similarly, cyclometalating ligand **4** was also obtained through both Mitsunobu and Suzuki-Miyaura reactions as shown in the Scheme [52]. The cyclometalating ligands (**2** and **4**) reacted with $K_2[PtCl_4]$ to afford the μ–chloro-bridged dimer complexes, following by a bridge-cleavage reaction with the β-diketonate [53] in the presence of Na_2CO_3 to yield the final complexes. The identity of the target complexes was confirmed by ^1H and $^{13}C\{^1H\}$ NMR spectroscopy and TOF-MS spectrometry.

As shown in Fig. S9 (Supporting information), thermogravimetric analysis (TGA) shows that both complexes have good thermal stability with a decomposition temperature (at 5% weight loss) of 320 °C for ***s*-Pt1** and 335 °C for ***s*-Pt2** (Table S1 in Supporting information). In order to explore the liquid crystal properties, the complexes were first studied using polarized optical microscopy (Figs. 1b-e). Complex ***s*-Pt1** melted on heating at 115 °C to form a SmA* phase before giving way to a chiral nematic phase at 123.5 °C, which cleared at 167.7 °C. As shown in Figs. 1b and c, on cooling the characteristic Grandjean texture of the N* phase and focal conic fan texture of the SmA* phase were seen clearly. Broadly analogous behavior was seen for ***s*-Pt2**, with an observed melting point of 150 °C, a SmA*-N* transition at 157.5 °C and clearing at 173.7 °C, although it is noted that in addition to the melting transition, there was an additional transition between two crystal phases at 75 °C. Again, characteristic textures for the N* (Fig. 1e) and SmA* phases (Fig. 1d) were formed on cooling.

From both microscopy and DSC (Fig. S10 and Table S1 in Supporting information), it was evident that neither complexed crystallized on cooling and indeed in the DSC thermogram for ***s*-Pt1**, there is evidence of a glass transition centered around 65 °C, although no such event is seen for ***s*-Pt2**. Interestingly, the clearing points of the two complexes are very similar, which points to the

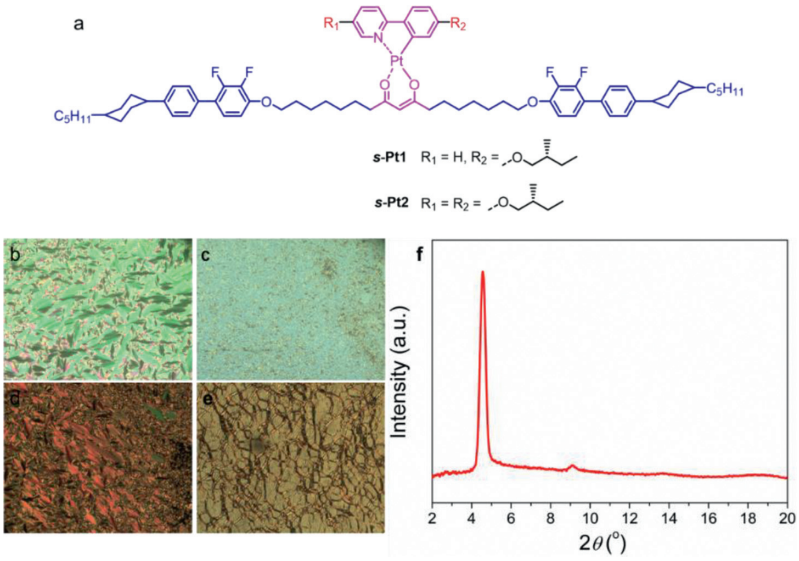

Fig. 1. Molecular structures (a); optical texture of ***s*-Pt1** (b and c at 120 and 160 °C, respectively) and ***s*-Pt2** (d and e at 149 and at 168 °C, respectively) on cooling, showing the SmA* phase (b, d) and chiral nematic phase (c, e) for each complex; (f) small-angle X-ray scattering for ***s*-Pt2** at 150 °C in the SmA* phase.

β-diketonate ligand driving the stability of the N* phase. However, the unsymmetric functionalization of the 2-phenylpyridine ligand in ***s*-Pt1** is evident in its lower melting point and SmA*-N* transition temperature.

Small-angle X-ray scattering data were collected in the SmA* phase of ***s*-Pt2** and are shown in Fig. 1f. Consistent with the lamellar nature of the SmA* phase, there is a strong (001) reflection at $2q = 4.55°$, corresponding to a layer spacing, $d(001)$ of 19.4 Å and there are weaker, higher-order reflections at $2q = 9.1°$ (002) and $2q = 13.7°$ (003) corresponding to spacings of 9.71 Å and 6.46 Å, respectively. Further, there is a weak feature at $2q = 18.6$ Å (4.59 Å), corresponding to the molten alkyl chains. In the N* phase at 165 °C, there is a broad reflection centered on $2q = 4.85°$ corresponding to a distance of 18.2 Å, which would normally be taken as representing the apparent length of the diffracting object (Fig. S11 in Supporting information). In Scheme S1, the complexes are drawn with the groups on the ancillary diketonate ligand in an extended all-*trans* arrangement. However, using data from a previous study [54] in which a single crystal structure was determined and where the same mesogenic group was used, the estimated length of ***s*-Pt2** in such an all-*trans* arrangement would be >60 Å. Compared with the observed layer spacing of *ca* 19.5 Å, there is a very significant shortening, which suggests that the actual configuration of ***s*-Pt1** and ***s*-Pt2** has the complex perhaps describing a U-shape. This would be achieved by the mesogenic groups folding round on themselves and generating a layered structure with very significant interdigitation. A similar arrangement has been proposed previously for LC-TADF materials that use the same mesogenic group [54].

Fig. 2a shows the UV-vis absorption and photoluminescent (PL) spectra of the platinum complexes in toluene solution and 10 wt% doped PMMA films at room temperature. The relevant photophysical data are summarized in Table S2 (Supporting information). Both complexes display analogous absorption spectra with three main absorption bands in toluene solution. The very strong absorption band at 280 nm is assigned to the $^1\pi$-π^* transition of the aryl ring moiety, while the intense absorption bands between 300 and 380 nm can be attributed to the singlet metal-to-ligand charge transfer transitions (^{1}MLCT). The very weak absorption bands between 380 and 450 nm originate from the triplet metal-to-ligand charge transfer transitions (^{3}MLCT) of the platinum 2-phenylpyridine complexes. At an excitation wavelength of 390 nm, both complexes present emission spectra with fine structured and with a visible shoulder at longer wavelength in the green-yellow region, implying that the emission mainly originates from the local excited (LE) state. Compared to ***s*-Pt1** (the emission peaks at 503 and 542 nm), ***s*-Pt2** exhibits a clearly red-shifted emission spectrum (the emission peak at 512 and 550 nm) owing to the presence of a second electron-donating oxygen from the alkoxy group. Impressively, the emission spectra of both complexes in doped PMMA film show negligible red shift compared to that in toluene solution, which can be explained by the suppressed intermolecular interaction in the solid state owing to a combination of the flexible chains and the polarity of PMMA film [55]. Compared to ***s*-Pt2**, interestingly, ***s*-Pt1** has a distinct aggregation emission at about 580 nm due to a different intermolecular interaction, seen also in the neat film and host matrix (PVK:OXD-7) (Fig. S12 in Supporting information).

The excited-state lifetime of the complexes was characterized by time-resolved emission at the excitation wavelength of 390 nm (Figs. 2b and c). Both complexes show a single exponential decay in the doped PMMA films with the emission lifetimes of 8.9 μs and 12 μs for ***s*-Pt1** and ***s*-Pt2**, respectively – typical for phosphorescence from a platinum(II) complex. Remarkably high photoluminescence quantum yields (PLQYs) were measured to be 85% and 78% for ***s*-Pt1** and ***s*-Pt2** in doped PMMA films.

To further explore the chiroptical properties of the metallomesogens, the circular dichroism (CD) spectra of ***s*-Pt1** and ***s*-Pt2** were acquired. Impressively, clear CD signal were detected (Fig. S13 in Supporting information) in toluene solution. Then, the circularly polarized luminescence (CPL) spectra and luminescence dissymmetry factor (g_{PL}) of the complexes were determined as neat films (Figs. 2d–g) and then doped in the PVK/OXD-7 host (Fig. S14 in Supporting information). Both complexes possess weak CPL signals with the g_{lum} values of 0.001 and 0.002 in the pristine films for ***s*-Pt1** and ***s*-Pt2**, respectively. Additionally, ***s*-Pt2** shows a stronger signal compared to ***s*-Pt1**, indicating that the additional chiral center can effectively amplify the g_{lum} factor of chiral emitters. To further explore the effect of liquid-crystallinity on CPL performance, the CPL signals and g_{lum} factor were measured with the annealed film of both platinum complexes. Impressively, intense CPL signals were detected and the g_{lum} values were both amplified by an order of magnitude, up to be 0.012 and 0.01 for ***s*-Pt1** and ***s*-Pt2**, respectively. This phenomenon can be ascribed to the higher-order orientation of the annealed film, which was caused by the liquid crystallinity. On the other hand, same phenomenon was observed

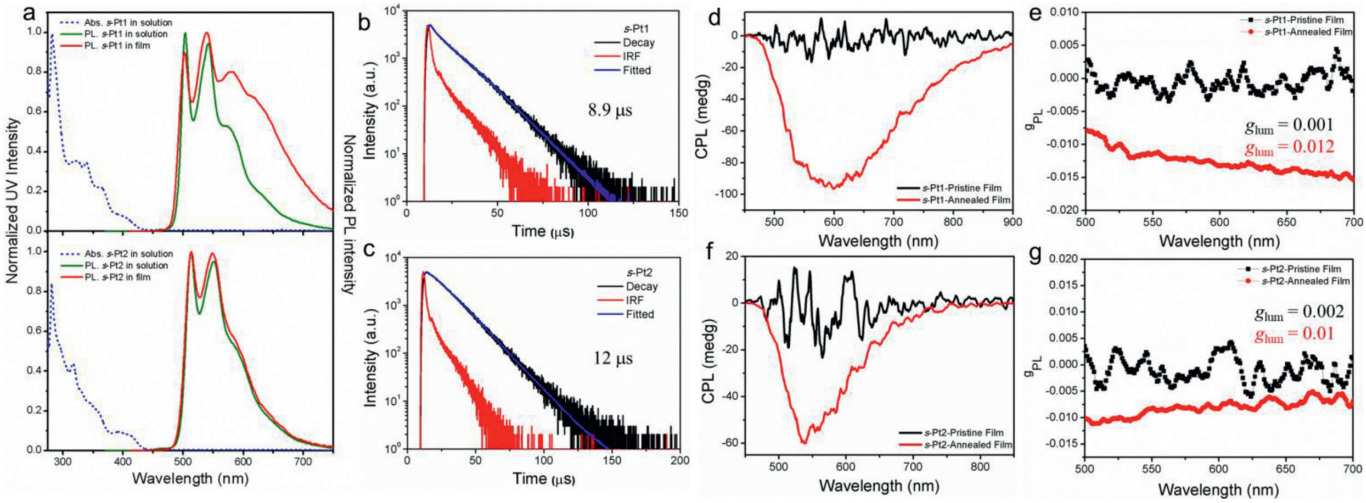

Fig. 2. Normalized UV absorption (dashed line) and PL spectra (solid line) of ***s*-Pt1** and ***s*-Pt2** in toluene solution and doped PMMA films (a). $\lambda_{ex} = 390$ nm. The concentration of solution is 10^{-5} mol/L. Time-resolved emission of ***s*-Pt1** (b) and ***s*-Pt2** (c) in doped PMMA films at 550 nm. CPL spectra of ***s*-Pt1** (d) and ***s*-Pt2** (f) in neat films before and after annealing process. The annealing temperature was 130 °C for D1 and 170 °C for D2, $\lambda_{ex} = 390$ nm. The g_{lum} value of ***s*-Pt1** (e) and ***s*-Pt2** (g) *versus* wavelength.

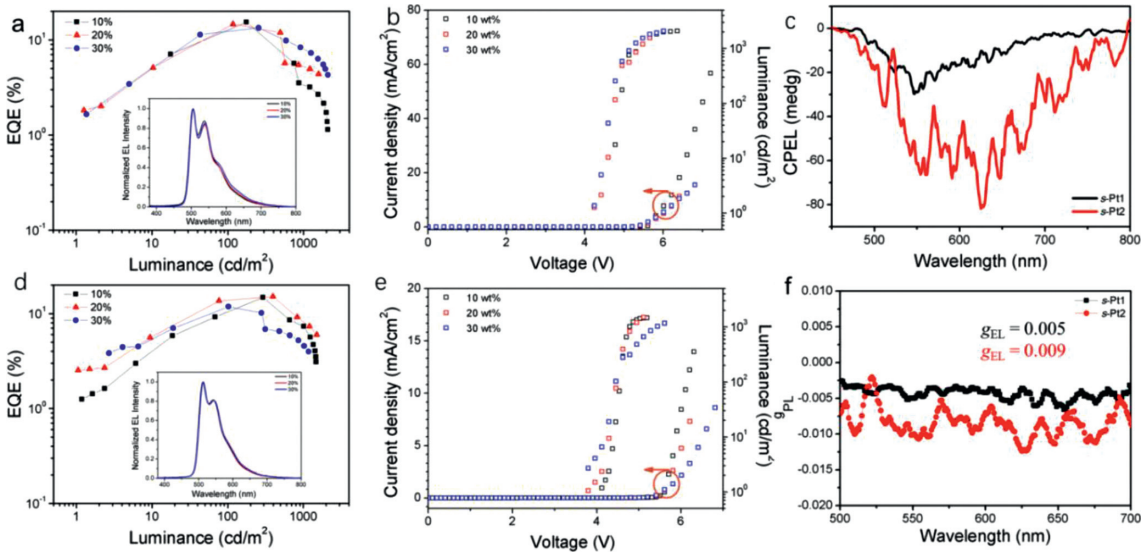

Fig. 3. Characteristics of CP-OLEDs based on ***s*-Pt1** and ***s*-Pt2** with different dopant concentrations. EQE-luminance curves of ***s*-Pt1** (a) and ***s*-Pt2** (d). Current density-voltage-luminance (*J-V-L*) curves of ***s*-Pt1** (b) and ***s*-Pt2** (e). CPEL spectra (c) and g_{EL} value (f) of CP-OLEDs based on ***s*-Pt1** and ***s*-Pt2**.

for both platinum complexes doped in the PVK/ OXD-7 host matrix (Fig. S14).

Cyclic voltammetry (CV) experiments were performed with the neat film in degassed CH_3CN solution (0.1 mol/L) to investigate the redox properties. As shown in Fig. S15 (Supporting information), an oxidation wave is observed at 1.01 and 1.03 V for ***s*-Pt1** and ***s*-Pt2**, respectively. Unfortunately, the reduction potential could not be detected below −2.0 V. Based on the empirical formulation of $E_{HOMO} = -(V_{OX} - V_{Fc/Fc+} + 4.8)$ eV, the highest occupied molecular orbital (HOMO) energy levels were calculated to be −5.35 eV for ***s*-Pt1** and −5.37 eV for ***s*-Pt2**. Accordingly, the lowest occupied molecular orbital (LUMO) energy levels were evaluated to be −2.36 eV and −2.71 eV for ***s*-Pt1** and ***s*-Pt2** according to their HOMO levels and optical bandgaps [56,57].

To explore the electroluminescent (EL) properties of the chiral complexes, solution processable circularly polarized OLEDs (CP-OLEDs) were prepared with the configuration of ITO/PEDOT: PSS (40 nm)/PVK: OXD-7: ***s*-Pt1**/***s*-Pt2** (10, 20, 30 wt%, 45 nm)/TmPyPB (40 nm)/LiF (1.2 nm)/Al (120 nm) (Fig. S18 in Supporting information).

As shown in Figs. 3b and d, both platinum complexes show structured EL emission profiles, similar to their PL spectra, implying that the emissions originate from the emitters. In addition, the host emission is absence in all the devices, which demonstrates complete energy transfer from the host matrix to the guest. In contrast to the case with many traditional square-planar platinum(II) complexes, excellent stable EL spectra were observed in these devices with varied dopant concentration. This phenomenon is due to the periphery flexible chains which can effectively suppress the intermolecular aggregation. Therefore, the Commission Internationale de lÉclairage (CIE) coordinates of the devices localize at (0.32, 0.59) for ***s*-Pt1** and (0.33, 0.61) for ***s*-Pt2** (Fig. S19 in Supporting information). Due to the concentration quenching, the ***s*-Pt1**-based devices achieved the optimum performance at the dopant concentration of 10 wt% with a maximum external quantum efficiency (*EQE*) of 15.3%, current efficiency (CE) of 49.3 cd/A and luminance (L) of 2087 cd/m^2 (Fig. 3 and Table S3 in Supporting information). In contrast, ***s*-Pt2** has a greater ability to suppress intermolecular interaction, which leads to the devices showed the best performance at 20 wt% dopant concentrations with a maximum *EQE* of 15.1%, a maximum current efficiency of 52.0 cd/A, and a luminance of 1504 cd/m^2.

In order to explore the circularly polarized electroluminescence (CPEL) properties of the devices, we investigated the devices with the dopant concentration at 20 wt% under an applied potential of 6 V. As shown in Figs. 3c and f, both devices show the clear CPEL signals similar with their corresponding CPL profiles, indicating the CPEL are from the chiral complexes. A g_{EL} value of 0.005 is observed for ***s*-Pt1**-based device, while the device based on ***s*-Pt2** exhibits much stronger CPEL intensity with a g_{EL} value of 0.009. Interestingly, the g_{EL} value of the ***s*-Pt2**-based device is almost twice than that of ***s*-Pt1**-based device, implying the number of chiral centers plays an important role on amplification the *g* value.

In summary, two chiral, platinum-based metallomesogens were prepared by including chiral centers and mesogenic units into cyclometalated platinum complex emissive core. The influence of liquid crystal properties and the number of chiral centers on chiroptic properties were investigated and both complexes were found to show a SmA* and a N* phase. Intense green emission was observed in solution and doped films for both complexes. Weak CPL were detected for complexes in neat film. However, after annealing process, both complexes showed enhanced CPL signals with a g_{PL} value of 0.012 for ***s*-Pt1** and 0.01 for ***s*-Pt2**. The solution-processed CP-OLEDs based on complexes achieved great device performance with a maximum EQE of 15.34% for ***s*-Pt1** and 15.11% for ***s*-Pt2**. Efficient CPEL were detected for the CP-OLEDs devices, since ***s*-Pt2** had two chiral centers, its g_{EL} value was almost twice that of ***s*-Pt1** with one chiral center. This research provided a strategy to enhance the luminescence dissymmetry factor of chiral luminescent materials in CP-OLEDs.

Declaration of competing interest

The authors declare that they have no known competing financial interests or personal relationships that could have appeared to influence the work reported in this paper.

Acknowledgments

The authors thank Professor Pengfei Duan, National Center for Nanoscience and Technology (NCNST), for measuring chiraloptical property and Dr. Stephen Cowling, University of York, for collecting the small-angle X-ray data for complex ***s*-Pt2**. Financial support was from the National Natural Science Foundation of

China (Nos. 51773021, 51911530197, 51473140), the Royal Society (IEC/NSFC/181139) and the National Natural Science Foundation of China (Nos. 51911530197 and 51773021) for an International Exchange Award (D.W. Bruce and Y. Wang) Six Talent Peaks Project in Jiangsu Province (No. XCL-102), Natural Science Fund for Colleges and Universities in Jiangsu Province (No. 19KJA430002), and Key technological tasks in Anhui Province (No. JB20007). The authors also would like to thank Analysis and Testing Center, NERC Biomass of Changzhou University for their help on NMR measurements.

Supplementary materials

Supplementary material associated with this article can be found, in the online version, at doi:10.1016/j.cclet.2022.107934.

References

[1] X. Wang, Y. Wang, W. Gao, et al., Adv. Mater. 33 (2021) e2003615.
[2] Y. Chen, P. Lu, Z. Li, et al., ACS Appl. Mater. Interfaces 12 (2020) 56604–56614.
[3] X. Zhan, F.F. Xu, Z. Zhou, et al., Adv. Mater. 33 (2021) 2104418.
[4] D. Li, G. Yu, Adv. Funct. Mater. 31 (2021) 2100550.
[5] J. Han, S. Guo, H. Lu, et al., Adv. Opt. Mater. 6 (2018) 1800538.
[6] D.W. Zhang, M. Li, C.F. Chen, Chem. Soc. Rev. 49 (2020) 1331–1343.
[7] L. Frederic, A. Desmarchelier, L. Favereau, G. Pieters, Adv. Funct. Mater. 31 (2021) 2010281.
[8] G. Albano, G. Pescitelli, L. Di Bari, Chem. Rev. 120 (2020) 10145–10243.
[9] F.S. Richardson, J.P. Riehl, Chem. Rev. 77 (1977) 773–792.
[10] E. Peeters, M.P.T. Christiaans, R.A.J. Janssen, et al., J. Am. Chem. Soc. 119 (1997) 9909–9910.
[11] S.Y. Yang, Y.K. Wang, C.C. Peng, et al., J. Am. Chem. Soc. 142 (2020) 17756–17765.
[12] D. Di Nuzzo, C. Kulkarni, B. Zhao, et al., ACS Nano 11 (2017) 12713–12722.
[13] L. Wan, J. Wade, F. Salerno, et al., ACS Nano 13 (2019) 8099–8105.
[14] D.M. Lee, J.W. Song, Y.J. Lee, C.J. Yu, J.H. Kim, Adv. Mater. 29 (2017) 1700907.
[15] J.H. Jung, D.M. Lee, J.H. Kim, C.J. Yu, J. Mater. Chem. C 6 (2018) 726–730.
[16] M. Li, M.Y. Wang, Y.F. Wang, L. Feng, C.F. Chen, Angew. Chem. Int. Ed. 60 (2021) 20728–20733.
[17] F. Ni, C.W. Huang, Y. Tang, et al., Mater. Horiz. 8 (2021) 547–555.
[18] Z.L. Gong, X. Zhu, Z. Zhou, et al., Sci. Chin. Chem. 64 (2021) 2060–2104.
[19] H. Sakai, S. Shinto, J. Kumar, et al., J. Phys. Chem. C 119 (2015) 13937–13947.
[20] J. Han, S. Guo, J. Wang, et al., Adv. Opt. Mater. 5 (2017) 1700359.
[21] Y. Liu, L. Hua, Z. Zhao, et al., Adv. Sci. 8 (2021) 2101326.
[22] Z.P. Yan, X.F. Luo, W.Q. Liu, et al., Chem. Eur. J. 25 (2019) 5672–5676.
[23] C. Li, A.K. Harrison, Y. Liu, et al., Angew. Chem. Int. Ed. 61 (2022) e202115140.
[24] Z. Jiang, J. Wang, T. Gao, et al., ACS Appl. Mater. Interfaces 12 (2020) 9520–9527.
[25] L. Wang, H. Xiao, L. Qu, et al., Inorg. Chem. 60 (2021) 13557–13566.
[26] T. Imagawa, S. Hirata, K. Totani, T. Watanabe, M. Vacha, Chem. Commun. 51 (2015) 13268–13271.
[27] S. Feuillastre, M. Pauton, L. Gao, et al., J. Am. Chem. Soc. 138 (2016) 3990–3993.
[28] F. Song, Z. Xu, Q. Zhang, et al., Adv. Funct. Mater. 28 (2018) 1800051.
[29] S. Sun, J. Wang, L. Chen, et al., J. Mater. Chem. C 7 (2019) 14511–14516.
[30] Z.G. Wu, H.B. Han, Z.P. Yan, et al., Adv. Mater. 31 (2019) e1900524.
[31] G. Hong, X. Gan, C. Leonhardt, et al., Adv. Mater. 33 (2021) 2005630.
[32] J.R. Brandt, X. Wang, Y. Yang, A.J. Campbell, M.J. Fuchter, J. Am. Chem. Soc. 138 (2016) 9743–9746.
[33] Z.P. Yan, K. Liao, H.B. Han, et al., Chem. Commun. 55 (2019) 8215–8218.
[34] G. Lu, Z.G. Wu, R. Wu, et al., Adv. Funct. Mater. 31 (2021) 2102898.
[35] Z. Yang, Z. Mao, Z. Xie, et al., Chem. Soc. Rev. 46 (2017) 915–1016.
[36] X. Liang, Z.L. Tu, Y.X. Zheng, Chem. Eur. J. 25 (2019) 5623–5642.
[37] Y. Tao, K. Yuan, T. Chen, et al., Adv. Mater. 26 (2014) 7931–7958.
[38] T. Huang, W. Jiang, L. Duan, J. Mater. Chem. C 6 (2018) 5577–5596.
[39] M.Y. Wong, E. Zysman-Colman, Adv. Mater. 29 (2017) 1605444.
[40] J.M. Teng, Y.F. Wang, C.F. Chen, J. Mater. Chem. C 8 (2020) 11340–11353.
[41] Q. Xue, G. Xie, Adv. Opt. Mater. 9 (2021) 2002204.
[42] Z.P. Yan, T.T. Liu, R. Wu, et al., Adv. Funct. Mater. 31 (2021) 2103875.
[43] D.W. Zhang, J.M. Teng, Y.F. Wang, et al., Mater. Horiz. 8 (2021) 3417–3423.
[44] T.T. Liu, Z.P. Yan, J.J. Hu, et al., ACS Appl. Mater. Interfaces 13 (2021) 56413–56419.
[45] P. Xue, X. Wang, W. Wang, et al., ACS Appl. Mater. Interfaces 13 (2021) 47826–47834.
[46] Y. Xu, Q. Wang, X. Cai, C. Li, Y. Wang, Adv. Mater. 33 (2021) e2100652.
[47] E.M. Sanchez-Carnerero, A.R. Agarrabeitia, F. Moreno, et al., Chem. Eur. J. 21 (2015) 13488–13500.
[48] J.P. Riehl, F.S. Richardson, Chem. Rev. 86 (1986) 1–16.
[49] X. Wu, M. Zhu, D.W. Bruce, W. Zhu, Y. Wang, J. Mater. Chem. C 6 (2018) 9848–9860.
[50] X. Yang, J. Han, Y. Wang, P. Duan, Chem. Sci. 10 (2019) 172–178.
[51] G. Qian, X. Yang, X. Wang, et al., Adv. Opt. Mater. 8 (2020) 2000775.
[52] B. Yang, H. Ni, H. Wang, et al., J. Phys. Chem. C 124 (2020) 23879–23887.
[53] Y. Wang, C.P. Cabry, M. Xiao, et al., Chem. Eur. J. 22 (2016) 1618–1621.
[54] Y. Zhu, S. Zeng, B. Li, et al., ACS Appl. Mater. Interfaces 14 (2022) 15437–15447.
[55] Y. Liu, Z. Yin, X. Wang, et al., J. Mater. Chem. C 8 (2020) 8971–8979.
[56] C. Adachi, M.A. Baldo, M.E. Thompson, S.R. Forrest, J. Appl. Phys. 90 (2001) 5048–5051.
[57] S.M. Suresh, E. Duda, D. Hall, et al., J. Am. Chem. Soc. 142 (2020) 6588–6599.